



## OPEN ACCESS

## EDITED BY

Michael Ojovan,  
Imperial College London, United Kingdom

## REVIEWED BY

Charles M. Folden,  
Texas A and M University, United States  
Dmitry Marinin,  
Institute of Chemistry (RAS), Russia

## \*CORRESPONDENCE

Mathurin Robin,  
✉ robin@subatech.in2p3.fr

RECEIVED 06 March 2024

ACCEPTED 21 May 2024

PUBLISHED 17 June 2024

## CITATION

Robin M, Rivonkar A, Suzuki-Muresan T,  
Abdelouas A and Mokili M (2024), Optimized  
precipitation process for the treatment of  
radioactive effluents from Ni-alloy  
decontamination using a chemical oxidation  
reduction process.  
*Front. Nucl. Eng.* 3:1396821.  
doi: 10.3389/fnuen.2024.1396821

## COPYRIGHT

© 2024 Robin, Rivonkar, Suzuki-Muresan,  
Abdelouas and Mokili. This is an open-access  
article distributed under the terms of the  
[Creative Commons Attribution License \(CC BY\)](https://creativecommons.org/licenses/by/4.0/).  
The use, distribution or reproduction in other  
forums is permitted, provided the original  
author(s) and the copyright owner(s) are  
credited and that the original publication in this  
journal is cited, in accordance with accepted  
academic practice. No use, distribution or  
reproduction is permitted which does not  
comply with these terms.

# Optimized precipitation process for the treatment of radioactive effluents from Ni-alloy decontamination using a chemical oxidation reduction process

Mathurin Robin\*, Aditya Rivonkar, Tomo Suzuki-Muresan, Abdelouas Abdelouas and Marcel Mokili

Subatech Laboratory (IMT Atlantique, CNRS/IN2P3, Nantes University), Nantes, France

Nuclear power plays a major role in the generation of electricity with low carbon emissions. However, it generates significant amounts of radioactive waste, mainly from contaminated metallic components such as steam generators. Decontamination is essential for the safe handling and eventual recycling or disposal of these materials. Various decontamination techniques can be utilized but chemical processes are recommended for complex geometries such as the tubular parts of steam generators. COREMIX (Chemical Oxidation REDuction using nitric permanganate and oxalic acid MIXture) is a process that is similar to the CORD (Chemical Oxidation Reduction Decontamination) process currently utilized in the industry which involves dissolving the contaminated oxide layers from metallic surfaces. This process generates a large quantity of radioactive effluent that requires appropriate treatment. The objective is to reduce metallic concentration and the radioactivity by precipitating metals in solution as hydroxides  $M^{(m-n)}(\text{OH})_n$  (with  $m$  the oxidation number of the metal  $M$ ). The optimization of a two-step precipitation protocol is presented here, with a study of the contact time (1–24 h) and the reagents used (NaOH and KOH). The resulting precipitates from this process are characterized using several techniques (FTIR, TGA and XRD). Tests were conducted on surrogate samples to demonstrate the viability of the process on more complex samples. Finally, the optimized protocols were implemented on radioactive Ni-alloy samples. Decontamination factors were calculated portraying the efficiency of both the COREMIX and the subsequent two-stage precipitation process. Characterization of the sludge produced during the process shows that the precipitate obtained at pH 8.5 consists mainly of iron (III) oxide-hydroxides, whereas the precipitate obtained at pH 12 is mainly composed of manganese (II,III) oxide. The optimization steps show that the contact time during the first precipitation and the choice of precipitants does not influence the efficiency of the protocol while the destruction of oxalic acid proves to be critical to quantitatively precipitate chromium. Ultimately, the COREMIX process can effectively decontaminate contaminated Ni-alloy samples, removing between

12% and 14% of the contamination in each cycle. Decontamination of effluent using the precipitation protocol results in a very high decontamination factor of between 3000 and 6000.

#### KEYWORDS

decontamination technology, metallic radioactive waste, COREMIX, liquid effluent, precipitation

## 1 Introduction

Nuclear power generation is widely used as an energy source in many countries. However, a significant proportion of the existing nuclear capacity, more than 60%, is over 25 years old. In Europe, the situation is particularly pressing, as 90% of all nuclear reactors are set to be shut down by 2030 unless their operational lifespan is extended (Volk et al., 2018; European Commission, 2016). This upcoming decommissioning process necessitates effective decontamination technologies to minimize occupational exposures, reduce potential releases of radioactive materials, and enable component reuse or recycle (Hirose and McCauley, 2022; Hu et al., 2018; Baja et al., 2009; Murray, 1986).

Decontamination plays a crucial role in nuclear decommissioning activities, with the aim of mitigating radiation risks and optimizing the management of radioactive wastes. Various decontamination technologies have been developed and implemented to address these challenges. These technologies not only enhance workplace safety but also have implications for radioactive waste management by minimizing the generation of secondary waste and allowing for further processing (Valencia, 2012; Deng et al., 2020; Shelenkova and Kulagina, 2021). As a result of decontamination efforts, a wide range and significant quantities of secondary radioactive waste can be generated. Therefore, optimizing decontamination technologies is essential not only for radiation protection but also for efficient radioactive waste management while keeping in mind environmental and economic requirements. It is crucial to reduce the volumes of secondary waste generated and explore opportunities for further processing or disposal.

In industries and nuclear facilities, effective management and treatment of radioactive liquid effluents are vital to protect the environment and ensure worker safety. The Chemical Oxidation Reduction using nitric permanganate and oxalic acid MIXture (COREMIX) process involves a series of alternating steps to achieve decontamination. It is derived from the existing CORD (Chemical Oxidation Reduction Decontamination) process which has emerged as a promising technique for the decontamination of radioactive metals surfaces. In the first step of this process, permanganate ions ( $\text{MnO}_4^-$ ) are employed to oxidize the chromium oxide layer, resulting in the release of chromate ions. Potassium permanganate can be used as the source of permanganate ions, either in nitric acid media (referred to as nitric permanganate (NP) CORD) or in alkaline media with potassium hydroxide (referred to as alkaline permanganate (AP) CORD) (Radó et al., 2004; Wille et al., 1997; Tian et al., 2019). Another variation of the CORD process, known as HP CORD is typically used and involves the utilization of UV source and permanganic acid prepared from potassium permanganate using a strong acid cation resin (Demmer, 1994; Ocken, 1999). In the subsequent step, oxalic acid is introduced

to reduce the permanganate ions to aqueous  $\text{Mn}^{2+}$  ions and dissolve the iron (Fe) and nickel (Ni) from enriched oxide layer of the alloy surfaces. This multi-step process is repeated several times to ensure thorough decontamination (Tian et al., 2019; Ocken, 1999).

To highlight the differences between COREMIX and the CORD process, the COREMIX begins with NP oxidation instead of the use of HP and does not require use an UV source. Further, COREMIX leaves room for destruction of oxalic acid using hydrogen peroxide, referring to COREMIX-H process. It is possible to follow this oxalic acid destruction with the use of resins or by precipitation protocol (named as COREMIX-HP process) for trapping the radionuclides.

However, a significant challenge arises from the generation of liquid effluents during the COREMIX process, which involves various range of concentrations of radioactive metallic ions. Effective treatment methods are crucial to meet regulatory standards and prevent potential adverse impacts on human health and the environment. In order to reduce the volume of these effluents and limit the quantity of resin needed for their purification, a pre-treatment step involving the precipitation and co-precipitation of metal cations has been optimized in pH as described in a previous work (Rivonkar et al., 2022).

There are many techniques currently available for separating and purifying liquid waste such as evaporation, filtration, chromatographic resin, precipitation and more. Nowadays, extraction by chromatographic resin is mainly used thanks to its high separation efficiency for a wide range of elements and complexes (Qi, 2018). However, this technique is relatively expensive because of the specificity and complexity of the resins used. One of the ways to reduce the amount of resins, and therefore the cost of treatment, is to pre-treat liquid waste upstream with, for example, a precipitation step.

The physico-chemical precipitation process is widely utilized for the treatment of metallic effluents, especially in the metallurgical and coal mine industries (Mishra and Das, 1992; Cravotta, 2008). In this method, a precipitant is introduced into the effluent solution, resulting in the formation of non-soluble metal precipitates. One method involves the addition of sodium hydroxide (NaOH) in multiple steps to precipitate the metals as hydroxides  $\text{M}^{(m-n)}(\text{OH})_n$  (with  $m$  the oxidation number of the metal  $M$ ). After separating the liquid phase from the solid precipitate, the precipitate can be incorporated in a suitable matrix, while the remaining solution can be treated using ion exchange resins (IAEA, 1992; Fu and Wang, 2011; Oncel et al., 2013). The hydroxide precipitation process holds numerous advantages when applied to the treatment of liquid effluents generated by the COREMIX process. Firstly, it offers a cost-effective approach to the removal of radioactive metals, taking advantage of its proven efficiency in removing metals from a wide range of industrial effluents. Moreover, this process demonstrates a high level of

selectivity, enabling the targeted removal of specific metal ions while minimizing the interference caused by other non-radioactive contaminants.

This article explores the fundamental principles of the hydroxide precipitation technique, focusing on factors that affect precipitation efficiency, such as pH, contact time and reactant concentrations. This study also focuses on the characterisation of the precipitates produced in order to better design the best possible conditioning matrix. In addition to discussing the theoretical aspects, this work addresses practical considerations related to implementing hydroxide precipitation for treating the effluent of the optimized and modified NP-CORD process (Rivonkar et al., 2022), now known as COREMIX. This includes an examination of potential challenges arising from the presence of complexing agents and competing ions, along with strategies to overcome these obstacles. Finally, the process will be applied to radioactive Ni-alloy samples decontaminated by the COREMIX process. Indeed, this process is particularly suitable for decontaminating metals with complex geometries, such as the tubular part of steam generators, made of stainless steel or Ni-alloy. This is why these metals were chosen as surrogate and radioactive samples for this study.

The findings of this study are expected to provide valuable insights into the efficiency of the hydroxide precipitation process for treating liquid effluents contaminated with radioactive metals from the COREMIX process. The result will contribute to the development of efficient and sustainable strategies for managing radioactive waste, particularly within the nuclear industry. Ultimately, this research aims to enhance the environmental sustainability and safety of nuclear waste treatment practices while reducing costs and therefore, further advancing the goal of responsible nuclear waste management. This includes incorporating the Life Cycle Assessment (LCA) (Muralikrishna and Manickam, 2017; Sphera, 2020; Guidi et al., 2010) and Life Cycle Costing (LCC) (Giorgi et al., 2019; European Commission, 2014) into analytical development in compliance with the Waste Acceptance Criteria (WAC) set by the European Union (IAEA, 1983; EURAD, 2020) and therefore promoting the concept of a circular economy (Ellen MacArthur Foundation, 2020; Geissdoerfer et al., 2020).

## 2 Materials and methods

### 2.1 Materials

#### 2.1.1 Metallic samples

The stainless steel surrogates samples mentioned in this article were the subject of a previous publication on the optimization of the COREMIX process (Rivonkar et al., 2022). As a reminder, these samples are 1 cm<sup>2</sup> 316Ti stainless steel specimens that were pre-oxidized using water and boric acid vapor by SORC (Hungary), in order to simulate the corrosion produced in steam generator pipes. The previous characterisation of these samples provides a better understanding of the composition of the surrogate effluents used in this study.

The two radioactive samples are metal parts made of Ni-alloy 600. Their dimensions were measured using a vernier caliper and set to 7.7 mm × 5.2 mm × 2.1 mm (length × width × thickness) for the

first sample (named M1) and 7.5 mm × 5.8 mm × 2.1 mm for the second one (named M2). The initial masses of these samples are 431 and 489 mg respectively. The initial radiological characterization of the Ni-alloy 600 M1 is detailed in Table 1.

The chemical composition of the stainless steel and Ni-alloy samples are given in Table 2.

#### 2.1.2 Liquid effluents

In this study, three types of effluents were used to develop and optimized the precipitation process involved after the COREMIX process: synthetic, surrogate and radioactive. Details of the effluents used in this study are given in Table 3. This includes the name of each sample, its type, chemical composition and volume.

The synthetic solution used in the optimisation part were prepared by dissolving metallic salts in 400 mL of water. This solution was previously acidified with 70% HNO<sub>3</sub> in order to obtain an acid solution, close to the final pH obtained after decontamination by the COREMIX process. Synthetic sample S1 was prepared by dissolving 480 mg of manganese dichloride (dihydrate, 99%, Merck); 740 mg of nickel nitrate (hexahydrate, 99%, Merck); 3.5 mg of cobalt (II) chloride (hexahydrate, 98%, Sigma-Aldrich); 100 mg of iron (III) chloride (hexahydrate, 98%–102%, Sigma-Aldrich); 160 mg of chromium (III) nitrate (nonahydrate, 99%, Acros Organics) and 170 µg of cerium (III) nitrate (hexahydrate, 99%, Sigma-Aldrich). For zinc, 2.5 mg/L is added using a standard solution for ICP-MS analysis (1,000 µg/mL, 99.99%, SCP Science). The final concentrations of metals were selected to depict their concentrations as if 1 g of metal was completely dissolved into the solution, whereas the amount of manganese arises from that added during the COREMIX process. After dissolution, the 400 mL solution was divided into two identical 200 mL samples named S1 and S2.

As for the surrogate effluents, they were generated during the treatment of oxidized stainless steel samples by the COREMIX process. They are mainly composed of nickel, iron and chromium from the steel dissolution. A significant amount of manganese is also present due to the use of KMnO<sub>4</sub> in the COREMIX process. Three different solutions named G1, G2 and G3 were used to optimized the oxalic acid destruction step (G1 and G2) and to study the influence of the precipitant used during the precipitation (G2 and G3).

The last type of effluent (radioactive) came from the decontamination of a radioactive Ni-alloy 600 sample by the COREMIX process. The decontamination factor of the precipitation process was estimated using two radioactive sample, R1 and R2.

### 2.2 Characterization

#### 2.2.1 Liquid characterization

The efficiency of the processes, specifically the dissolution of the oxide layer using the COREMIX process and the removal efficiency of metallic ions through the precipitation process, was evaluated by measuring the concentrations of dissolved metals using Inductively Coupled Plasma Mass spectroscopy (X-Series II, Thermo Electron). Analytical uncertainties are estimated to be ±10%. <sup>45</sup>Sc and <sup>115</sup>In were utilized as internal standards. A SCP Science multi-element

TABLE 1 Gamma radiological characterisation of radioactive Ni-alloy 600 sample M1.

Radionuclide	Energy emission	Intensity	Average activity
	keV	%	(Bq/g)
<sup>54</sup> Mn	834.85	99.98	150 ± 30
<sup>57</sup> Co	122.06	85.51	13 ± 8
<sup>60</sup> Co	1,173.2	99.90	32,000 ± 1800
	1,332.49	99.98	
<sup>125</sup> Sb	427.87	29.55	110 ± 40
	463.36	10.48	
	600.6	17.76	
Total (Bq/g)			32,300 ± 1800
Total (Bq)			13,900 ± 800

TABLE 2 Chemical composition of the metallic samples (wt%).

Type of metal	C	Si	S	Cr	Ni	Mn	Cu	Fe	Mo
Ni-alloy 600	≤ 0.15	≤ 0.5	≤ 0.015	14–17	≥72	≤ 1	≤ 0.5	6–10	-
Stainless Steel 316Ti	≤ 0.08	≤ 1	≤ 0.03	16–18	10–14	-	-	Balance	2–2.5

TABLE 3 Chemical composition of the liquid effluents.

Sample			Concentration (mg/L)							Volume (mL)
Experiment	Type	Name	Cr	Mn	Fe	Co	Ni	Zn	Ce	
Characterization (§3.1)	Synthetic	S1	136	829	838	2.3	175	2.9	0.8	200
Time of contact (§3.2.1)		S2								
Oxalic destruction (§3.2.2)	Surrogate	G1	0.7	43	7.7	-	0.4	-	-	250
		G2	1.2	412	5.4	-	0.8	-	-	250
Precipitant (§3.2.3)		G3	2.8	412	12.3	-	3.8	-	-	300
Implementation (§3.3.2)	Radioactive	R1	0.8	413	0.8	-	3.9	-	-	350
		R2	0.8	322	2.1	-	3.4	-	-	350

standard was used to establish the calibration curves before each analysis.

## 2.2.2 Solid characterization

### 2.2.2.1 FT-IR

Invenio-S Fourier Transform InfraRed spectroscopy (FTIR) spectrometer (Bruker) was used to characterize the sludge generated during the effluent treatment process. Measurements were taken according to the attenuated total reflectance (ATR) of few milligrams of samples with a diamond crystal at wavelengths ranging from 400 to 4,000 cm<sup>-1</sup> in steps of 1.43 cm<sup>-1</sup>.

### 2.2.2.2 TGA/DSC

Thermogravimetric analysis of the samples were carried out using Setsys Evolution 16/18 TGA-DSC (SETARAM). TGA/DSC

measurements were done on 15–20 mg of sample with a linear temperature increase of 10 °C/min until a temperature of 950 °C is reached. The initial sample temperature is fixed at 25 °C before launching the analysis. The heat flow, the mass of the sample and the derivative of the mass as a function of time were monitored during the analyses.

### 2.2.2.3 XRD

X-ray diffraction analysis was carried out using the D8 Advance, XRD device (Bruker) under the following conditions: 10°–70° 2theta, a step size of 0.01°, and a scan speed of 2 s/step. The patterns were analyzed by Diffrac Eva software (Version 4.3.1.2, Bruker) using the Crystallography Open Database (Rev 173,445). As the quantity of sample analyzed is very small, the holder used for the analysis is a thin glass slide to avoid any pollution of the pattern that might be

caused by the diffraction of HDPE support. An anti-scatter knife edge was used to reduce the background scattering at low angles.

#### 2.2.2.4 Mass loss corrosion rate

Estimating the corrosion rate can be achieved by analyzing the mass loss experienced during the treatment process (Malaret and Yang, 2022; Kutz, 2005). This parameter can be used to compare the efficiency of the two processes (CORD and COREMIX) on radioactive Ni-alloy samples. The average corrosion rate (CR) can be estimated using the equation:

$$CR = \frac{m_{\text{loss}}}{A \cdot t \cdot \rho} \quad (1)$$

The corrosion rate (CR) given by the Eq 1 is expressed in micrometers per hour ( $\mu\text{m/h}$ ). The mass loss of the metal, denoted as  $m_{\text{loss}}$  in grams (g), is calculated as the difference between the initial mass ( $m_0$ ) and the final mass ( $m_t$ ) during a specific contact time,  $t$ , measured in hours. The surface area of the material exposed to corrosion, denoted as  $A$ , is measured in square centimeters ( $\text{cm}^2$ ), while the density of the material, represented by the symbol  $\rho$ , is measured in grams per cubic centimeter ( $\text{g/cm}^3$ ).

### 2.2.3 Radiological characterization

#### 2.2.3.1 Gamma spectrometry

Gamma spectrometry was conducted using a High Purity Germanium (HPGe) detector housed in a low-background lead castle. The GENIE 2000 software was used for spectrum analysis, while LABSOCS from Mirion-Canberra was used for geometry modeling. For the solid Ni-alloy samples used in the COREMIX process, simplified box geometry templates were utilized, and their dimensions were adjusted to match the sample sizes, disregarding any curvature resulting from the tubes. The sample was of Ni-alloy 600 with a composition as in Table 2. The theoretical density of Ni-alloy 600,  $8.47 \text{ g/cm}^3$  was utilized (Special Metals, 2008).

To model the oxide layer on the inner surface of the samples, an average thickness of  $2 \mu\text{m}$  was adopted based on measurements from surrogate samples. The composition of this oxide layer was assumed to be a mix of  $\text{Fe}_2\text{O}_3$  and  $\text{Fe}_3\text{O}_4$ . As the density of these two compounds is close ( $5.24$  and  $5.17 \text{ g/cm}^3$ ), a rounded value of  $5 \text{ g/cm}^3$  was chosen to model the oxide layer. It was observed that the density had negligible influence on the results at this thickness. During the solid characterization, the samples were placed in plastic Petri dishes included in the LabSOCS model as a shielding component. The count time for gamma spectrometry analysis of the solid Ni-alloy samples was set to 30 min.

For the liquid solutions, standard 50 mL HDPE tubes were employed, and their geometry was pre-defined in the LabSOCS software. During the permanganate step of the COREMIX process, a volume of 5 mL of solution was used. This minimal volume was chosen to ensure that the COREMIX process was not disrupted. In the oxalic acid stage, a volume of 50 mL of solution was utilized. The count time for gamma spectrometry analysis of the liquid solutions was set to 2 h.

During the precipitation steps, gamma spectrometry of liquid solutions was done at each step of the process: initial, after destruction of oxalic acid, after first precipitation and after second precipitation. The measurements were done with a volume of 50 mL in a standard 50 mL HDPE tubes for a count time of 8 h. The count time for the solution after second

precipitation was increased to 24 h due to its low activity. The precipitates obtained during the two steps were also subject to gamma spectrometry after air drying for 3 days. To model the precipitate produced, a thickness of 0.1 mm was defined and the density of the first precipitate was set to  $3.12 \text{ g/cm}^3$ , which corresponds to the density of the main component,  $\text{Fe}(\text{OH})_3$  (Haynes, 2006). Likewise for the second precipitate the density was set to  $4.84 \text{ g/cm}^3$ , i.e., the density of manganese oxide  $\text{Mn}_3\text{O}_4$  (Haynes, 2006). The counting time was also identical as the Ni-alloy sample and set at 30 min.

#### 2.2.3.2 Dose rate detection

The dose rate of the sample was measured using four different handheld instruments. They were:

1. COLIBRI Survey Meter: Designed to detect and measure gamma radiation using a ionization chamber for detection. The COLIBRI used during this project can measure from  $10 \text{ nSv/h}$  to  $1 \text{ mSv/h}$  (Mirion Technologies, 2021).
2. 6150 AD-6 Portable Radiometer: Intended for measuring gamma and X-ray radiations. The average dose rate is measured and constantly updated during the measurement phase (Saphymo, 2015).
3. Gamma and X-Ray Probe: The gamma and X-ray dose were measured using NaI scintillator Gamma and X probes (ICTO probes, Carmelec) connected to a poly-radiometer (ICTO, Carmelec).

The decontamination factors were determined using the reduction in dose rates for each instrument, and an average was taken to obtain the total decontamination factor.

#### 2.2.3.3 Liquid scintillation

The global radioactivity of the Ni-alloys samples was measured by liquid scintillation on the Tricarb 3170-TR-SL liquid scintillation counter (Perkin Elmer). A study of the stability of the scintillating liquids (cocktails) was carried out prior to the analysis in order to establish the optimum mixture to use for analysing the active samples. Two different cocktails were tested, Ultima Gold LLT and Ultima Gold AB (Perkin Elmer). These were mixed with aqueous solutions at different pH levels (4, nine and 12) and their development was monitored visually for up to 30 h to observe the potential appearance of precipitates, phase separation, colouration or opacity. Ultima Gold AB transformed into white and fairly opaque solution, making it impossible to use. Ultima Gold LLT was selected as there was no transformation observed during the entire duration of observation.

For the measurements, the sample was mixed with Ultima Gold LLT (1:9 ratio). The acquisition time was set to 1 hour per tube and divided into three channels: 0–75 keV, 75–300 keV, 300–2000 keV. The counts detected from the three channels were summed and compared to deduce the global decontamination factors across solutions.

## 2.3 COREMIX process

The COREMIX process is based on an optimized 2-step NP CORD process (now renamed as COREMIX). Details of the process

are found in (Rivonkar, 2023) and the main steps are presented here in brief. The first step utilized 50 mL of 15 mM of potassium permanganate (ACS reagent,  $\geq 99.0\%$ , Merck) solution in the presence of 3 mM of nitric acid (70%, ACS reagent, Fisher Chemical). This step was applied for 3 h at  $80^\circ\text{C}$  and was followed by addition of 50 mL of oxalic acid (dihydrate, ACS reagent,  $\geq 95.0\%$ , Alfa Aesar) to give a final concentration of 18.5 mM oxalic acid at 100 mL. This step, lasted for 3 h at  $80^\circ\text{C}$ , is responsible for the decontamination step and the destruction of  $\text{MnO}_2$  generated (Wang and Stone, 2006; Ocken, 1999).

The process mentioned above was applied to radioactive sample M1 and M2. Four cycles ( $\text{KMnO}_4 + \text{H}_2\text{C}_2\text{O}_4$ ) were carried out to decontaminate these samples, estimate the repeatability of the process and to calculate a decontamination factor. In addition to this, a fifth cycle was then added to test the influence of different parameters on the decontamination factor per cycle.

For this purpose, the fifth cycle of sample M1 was performed with a higher concentration of oxalic acid (27.5 mM instead of 18.5 mM). On the other hand, the fifth cycle of sample M2 was performed with a longer contact time (6 h instead of 3 h). These tests were done to assess the effect of concentration and contact time on the decontamination of the Ni-alloy 600 sample.

## 2.4 Optimization of effluent precipitation

The precipitation protocol which follow the COREMIX process was already applied and tested on a synthetic sample (Rivonkar et al., 2022). This test was carried out after modelling the solubility of the metal hydroxides of interest using PhreeqC software. Based on these results, a precipitation protocol was developed. It includes an initial precipitation at pH 8.5 by adding 1M NaOH (Titrisol, Merck Supelco) to remove Fe, Cr and Zn. After filtration of the resulting sludge, a second precipitation was carried out at pH 12 to remove the remaining metals Mn, Ni and Co.

The various optimization and application tests carried out subsequently are based on this pH-optimized protocol. Prior to implementing this protocol on the radioactive active sample of Ni-alloy 600, different parameters of the protocol were investigated and a study of the solid generated was performed.

First of all, characterization studies by FTIR, TGA and XRD were carried out on the sludge generated after the precipitation of the synthetic sample S1, in order to establish its precise composition with a view to subsequent appropriate conditioning. For the liquid part, not all the metal cations precipitate at pH 8.5, which is why the precipitation kinetics were studied with the aim to determine whether the stirring time played a role in the efficiency of this reaction.

Then, the NaOH solution used to adjust the pH provides a large quantity of sodium salts which must be eliminated at the end of the effluent purification process. At the same time, the COREMIX process introduces potassium salts into the effluent due to the use of potassium permanganate ( $\text{KMnO}_4$ ). To reduce the number of different salts species to be treated by the ion exchange resins, tests were carried out by replacing sodium hydroxide with potassium hydroxide in the precipitation process.

Finally, adjustments had to be made to match the treatment conditions used by the COREMIX process, in particular by destroying the oxalic acid present in excess in solution.

### 2.4.1 Effect of stirring time

To test the precipitation kinetics, a synthetic solution (S2) was made by dissolving metal salts in 200 mL of acidified water. Once all the salts have been dissolved, the solution is stirred and the pH is increased by progressively adding 1 M NaOH with a titration device (716 DMS titrino, Metrohm) and a pH meter (Solitrode Pt1000, Metrohm) until the desired pH was reached. When pH 8.5 is reached, the addition of NaOH is stopped and 5 mL of the solution is taken and filtered with a syringe filter (cellulose acetate,  $0.45 \mu\text{m}$ , Sartorius) after being left to stir for 1, 2, 4, 6, 8 and 24 h respectively. Each aliquot was stabilized with 10  $\mu\text{L}$  of 70%  $\text{HNO}_3$  to ensure no further precipitation occurs and was placed inside a refrigerator. The analysis of these aliquots was made with inductively coupled plasma mass spectroscopy (ICP-MS).

### 2.4.2 effect of oxalic destruction

Once the protocol had been optimized in pH and contact time, tests were carried out on two surrogate effluents (G1 and G2). The effluents are coming from stainless steel 316Ti pieces that were treated identically using three cycles of the optimized COREMIX process, and the liquid wastes generated during the process were collected and mixed for a total of 250 mL each.

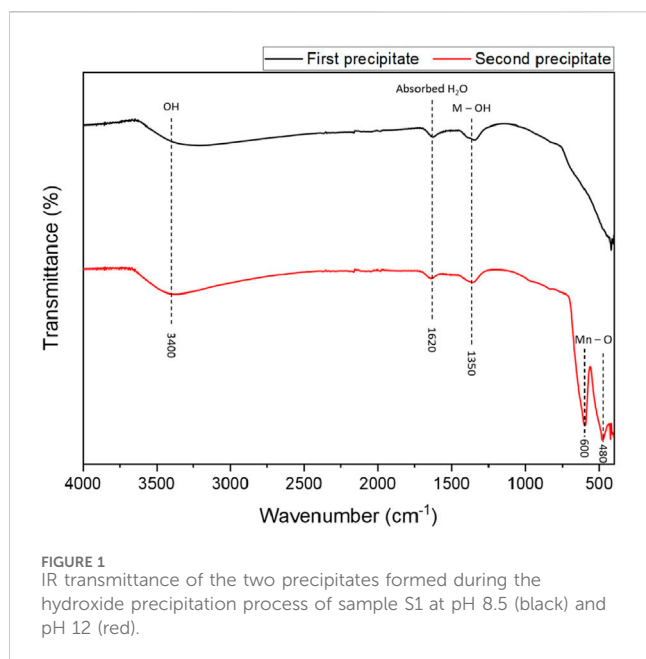
Two surrogate samples of stainless steel 316Ti were treated identically using three cycles of the optimized COREMIX process, and the liquid wastes generated during the process were collected and mixed for a total of 300 mL each. One effluent (G1) was treated by the precipitation protocol using 12.0 mL of 1 M NaOH. The other effluent (G2) was first heated to  $80^\circ\text{C}$  for 48 h with a heating stirring plate with 30.6 mL of  $\text{H}_2\text{O}_2$  (30% in water, Thermo Fischer) in order to destroy the excess oxalic acid. These parameters were found optimal for destruction of low concentrations of oxalic acid without the use of UV light (Blenkinsop et al., 2024). Following this pre-treatment step, the precipitation protocol is applied with a total of 5.3 mL of 1 M NaOH and all the solutions are analyzed by ICP-MS. The results from the two different effluents are then compared to observe the influence of excess oxalic acid before the precipitation.

### 2.4.3 Effect of precipitant

To test the effect of precipitant, 1 M solution of KOH was prepared using KOH pellets ( $\geq 85\%$ , Fischer) dissolved in deionized water. This solution was used to raise the pH of the effluent G3, produced during the decontamination of a piece of stainless steel by the COREMIX and acid oxalic destruction process (COREMIX-H). 1.9 mL of KOH were used to raise the pH to 8.5 before adding a further 0.6 mL to raise the pH to 12. The results of ICP-MS measurements were compared to those for experiments using NaOH previously with sample G2.

## 2.5 Implementation on radioactive samples

Implementation of the full decontamination protocol (COREMIX-HP) was carried out to evaluate its efficiency



(decontamination factor) on radioactive samples (M1 and M2) made of Ni-alloy 600.

The two steps of the COREMIX process explained in Section 2.3 were conducted in 125 mL heat-resistant glass beakers (Le Parfait Super Jars). These beakers were chosen for their wide openings, facilitating easy sample insertion, and secure sealing capabilities to prevent volume loss at elevated temperatures. The temperature rise was achieved by placing the jar in a climatic test chamber (Thermotron, INFORS HT) for simultaneous heating and agitation at speeds of up to 80 rpm. At the end of each step, 5 mL aliquot was taken for ICP-MS analysis, therefore leading to two aliquots taken for each cycle. Each aliquot was acidified by adding nitric acid to maintain the stability of dissolved metals. A total of four identical cycles were employed for both the samples. The fifth cycle was used to test different conditions in order to improve the decontamination rate. The details of this specific cycle are given in part 2.3.

For the subsequent precipitation protocol, solutions from only the first four cycles were utilized. The effluents generated by the sample M1 were collected in a 1 L glass beaker (Le Parfait Super Jars) and the resulting 350 mL solution was named R1. The same thing was done with sample M2 to create the sample R2. The oxalic acid destruction was performed in the climatic test chamber set up at 80 °C, 80 rpm for 48 h. The solutions are then left to cool down before adjusting the pH by adding 1 M KOH. After reaching pH 8.5, stirring is maintained for 1 h and stopped to allow the solid phase to settle. This allows for time savings during filtration by avoiding the clogging of the filter at the start of filtration. The filtration is made under vacuum (160 mbar) with a 0.2 μm acetate cellulose filter and air-dried afterward. The second precipitation is followed by adjusting the pH to 12. After each step of the process, two 5 mL aliquots were taken for ICP-MS and liquid scintillation measurements. A further aliquot of 50 mL was collected for gamma characterization and returned to the solution after analysis.

The results relating to the decontamination of sample R1 are presented and detailed in this article. Sample R2, which was used to test the repeatability of the experiment, is described in detail in the [Supplementary Material](#).

## 3 Results and discussion

### 3.1 Characterization of precipitated sludge

#### 3.1.1 FTIR

The FTIR characterization of the two precipitates generated during the tests on synthetic sample S1 are presented in Figure 1. The measurements were done according to the transmittance of the samples. The black line corresponds to the first precipitate obtained at pH 8.5 whereas the red one refers to the precipitate formed at pH 12. They were both dried at 40 °C for 48 h in an oven before analysis.

The two spectra are very similar and both show a broad and weak peak centered around 3400 cm<sup>-1</sup> which corresponds to the stretching vibrations of the O-H bonds in the hydroxyl groups on the surface and hydrogen-bond surface group according to Seehra et al. (2004), Shahadat et al. (2013). The peak visible at 1,620 cm<sup>-1</sup> is in line with this statement as it represents absorbed H<sub>2</sub>O (Nasrazadani, 1997).

The last peak at 1,350 cm<sup>-1</sup>, which is visible on both spectra, is observed by Laversin (Laversin, 2006) as a bending vibration of Fe-OH bond. As iron is mainly contained in the first precipitate, it is not expected to be visible in the spectrum of the second precipitate where manganese should be. One explanation may come from observations made by Perachiselvi et al. (Perachiselvi et al., 2020) where a similar peak, defined as O-H bending vibration combined with Mn atoms was observed when analyzing manganese (Mn<sub>3</sub>O<sub>4</sub>) particles. The authors found two peaks at 480 and 600 cm<sup>-1</sup>, identified as the vibration modes of tetragonal and octahedral Mn-O bonds. These two signature peaks of this structure are also visible in the studies carried out by Durmus et al. (2009), Chouchaine et al. (2022).

According to the results of the FTIR analysis, the metals contained in the precipitates appear to have bonded to the hydroxide ions, causing them to precipitate. The presence of metal-oxygen bonds and hydrogen bonds suggests that metal oxides or hydroxides have been formed, as expected. However, this hypothesis needs to be confirmed by other characterisation techniques.

#### 3.1.2 TGA/DSC

The two precipitates were also analyzed in TGA/DSC and the results are seen in Figure 2. Three parameters can be monitored as a function of sample temperature, the heat flow regarding the energy consumed or produced in blue, the mass loss in green and its derivative in time in pink.

The result for the sample analyzed after the precipitation at pH 8.5 is shown in Figure 2A. The heat flow shows several variations in energy, including two endothermic peaks at 138 °C and 222 °C and an exothermic peak at 520 °C. The two lowest energy peaks are supported by a sudden loss of sample mass of 3.7 g (21%) between 25 °C and 300 °C. These two effects can be linked with a loss of water

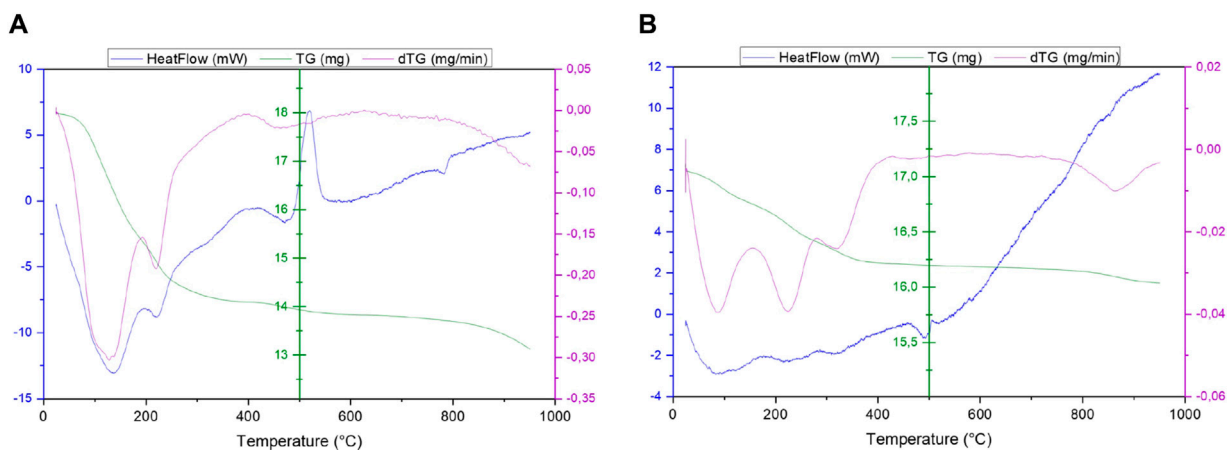


FIGURE 2 TG and DSC analysis of the (A) first and (B) second precipitate generated during the precipitation process of sample S1.

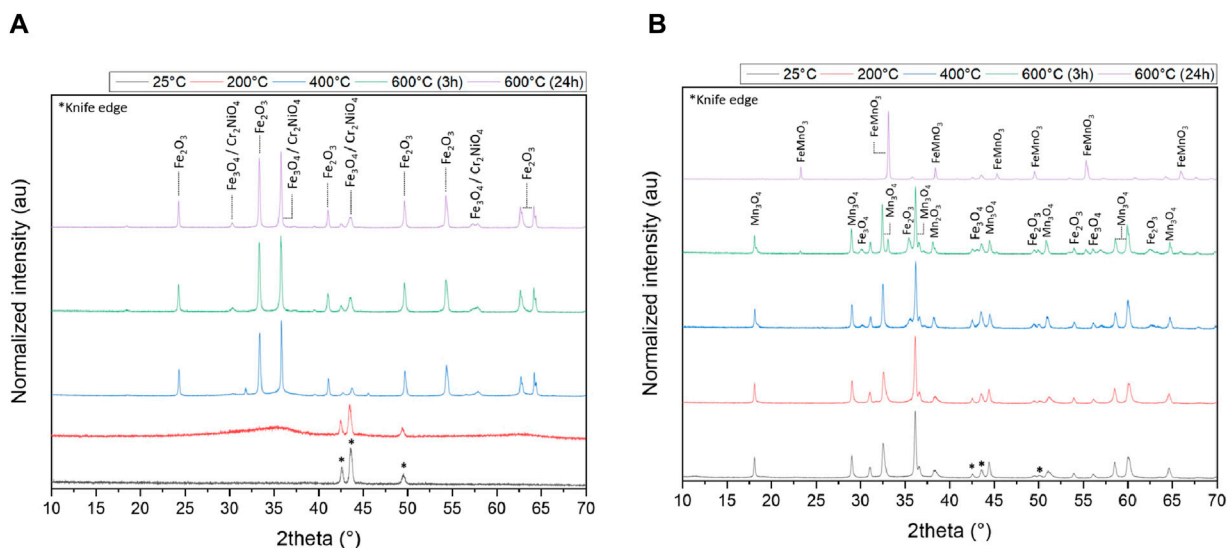


FIGURE 3 XRD diffractogram of the (A) first and (B) second precipitate generated during the precipitation process of sample S1, both normalized to the solid dried at 25°C.

molecules on the surface as it can be seen in the work of Vichery (2012).

These losses in mass and energy can also be explained by the appearance of a crystallization phenomenon. Indeed, the crystallization of iron complexes such as iron (III) hydroxide  $\text{Fe}(\text{OH})_3$  or iron (III) oxide-hydroxide  $\text{FeO}(\text{OH})$  slowly produce maghemite ( $\gamma\text{-Fe}_2\text{O}_3$ ) from 25°C to 300°C according to Balek (1995) and magnetite starting from 70°C to 80°C in alkaline and saline conditions for Taitel-Goldman (2015).

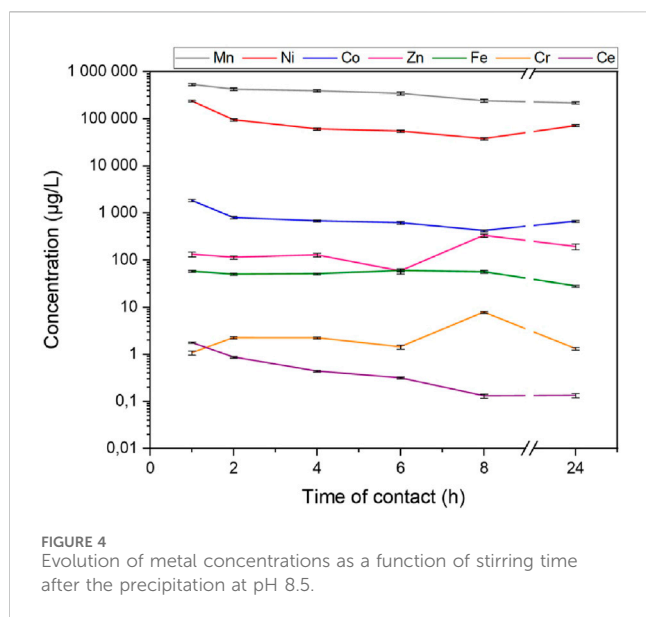
The last energy variation can be seen at 520°C, this peak is characteristic of the structural transformation of maghemite into hematite ( $\gamma \rightarrow \alpha\text{-Fe}_2\text{O}_3$ ) (Daou, 2007; Mürbe et al., 2008; Mazo-Zuluaga et al., 2003). This analysis suggests that the iron present in the solution is precipitated in hydroxyl form, which

subsequently crystallizes out as iron oxide as the temperature rises.

The second precipitate in another hand, has no endothermic peaks at low temperatures meaning that no crystallization takes place as the temperature of the solid rises. However, mass losses are still visible from mass derivative at 87°C and 225°C representing the loss of water molecules on the surface of the sample. The heat flux then gradually increases, which could be caused by a gradual change in chemical composition or structure.

### 3.1.3 XRD

Figure 3 shows the results of the characterization of the two precipitates by XRD analysis. The analysis was carried out on sludge dried at room temperature and after calcination of the samples to



200°C, 400°C and 600°C for 3 h, in order to observe the evolution of their chemical structure as a function of temperature and to validate the results obtained by TGA/DSC.

The XRD pattern of the first precipitate (Figure 3A) does not reveal diffraction peaks up to 200°C (except peaks coming from the knife edge tools), leading to the hypothesis that the solid generated is either amorphous or nano-crystallized. Few peaks are visible, but rather indicate diffraction from the sample holder or the beam knife, as they are present in all spectra and at the same intensity. After heating the sample to 400°C, the XRD profile shows various oxides as Fe<sub>2</sub>O<sub>3</sub>, Fe<sub>3</sub>O<sub>4</sub>, Cr<sub>2</sub>NiO<sub>4</sub>. The remarkable peaks of some of these oxides have also been observed in several studies on iron oxides (Bertolucci et al., 2015; Zainuri, 2017). Given the concentrations used to prepare the initial solution, iron oxides have been massively precipitated compared to chromium, nickel and zinc oxides. The same compounds are also present at 600°C after 3 and 24 h of calcination. These results are in agreement with those found in Section 3.1.2 (TGA/DSC) where the crystallization of a hydroxyl form of iron appears around 220°C.

Unlike the first analyzed sample, the second one generated during the precipitation at pH 12 shows peaks at room temperature (Figure 3B) similar to those from the study of Atique Ullah et al. (2017). Manganese (II, III) Mn<sub>3</sub>O<sub>4</sub> also known as MnO·Mn<sub>2</sub>O<sub>3</sub>, is a major component of this sample but other oxides can be found like Fe<sub>2</sub>O<sub>3</sub>, Fe<sub>3</sub>O<sub>4</sub> and Mn<sub>2</sub>O<sub>3</sub>. From 600°C, some peaks of FeMnO<sub>4</sub> start to appear after 3 h and are really intense after 24 h of heating.

Substitution of a manganese atom by an iron atom was also observed by Seifu et al. (2000) for similar temperatures who synthesized this oxide by mechanically alloying Fe<sub>2</sub>O<sub>3</sub> and Mn<sub>2</sub>O<sub>3</sub>. These characteristic peaks were also observed by Leontie et al. (2018). The other elements such as Ni, Ce, Co, Cr, Zn cannot be seen on this XRD pattern because of their low concentrations.

Regarding all the characterization results, it is possible to establish the hypothesis that the first precipitate obtained at pH 8.5 consists mainly of iron oxide-hydroxide (goethite). FTIR analysis highlights the presence of OH bonds, while the results

obtained from XRD and TGA/DSC show crystallization of the initial sample as iron oxide which may occur due to the low thermodynamic stability of hydrated iron (III) hydroxide (Cornell et al., 1989). As for the second precipitate generated at pH 12, the results obtained using the various measurement techniques indicate the presence of manganese oxide as the major component.

## 3.2 Optimization of effluent precipitation

### 3.2.1 Effect of stirring time

In order to study the effect of the stirring time of the solution during precipitation at pH 8.5, a study of the kinetics was carried out on the synthetic sample S2. The concentrations of the different metals in solution as a function of stirring time during the first precipitation of the protocol (pH 8.5) can be seen in Figure 4.

The results of this kinetic analysis show that the concentrations of metals do not vary significantly for compounds with high concentrations in the first hours after the pH adjustment. After 8 h of stirring, an increase in the concentration of Zn and Cr was observed, probably due to an experimental artifact during the ICP-MS measurements (contamination). In fact, the concentration of these two elements decreased between 8 and 24 h, as did that of manganese.

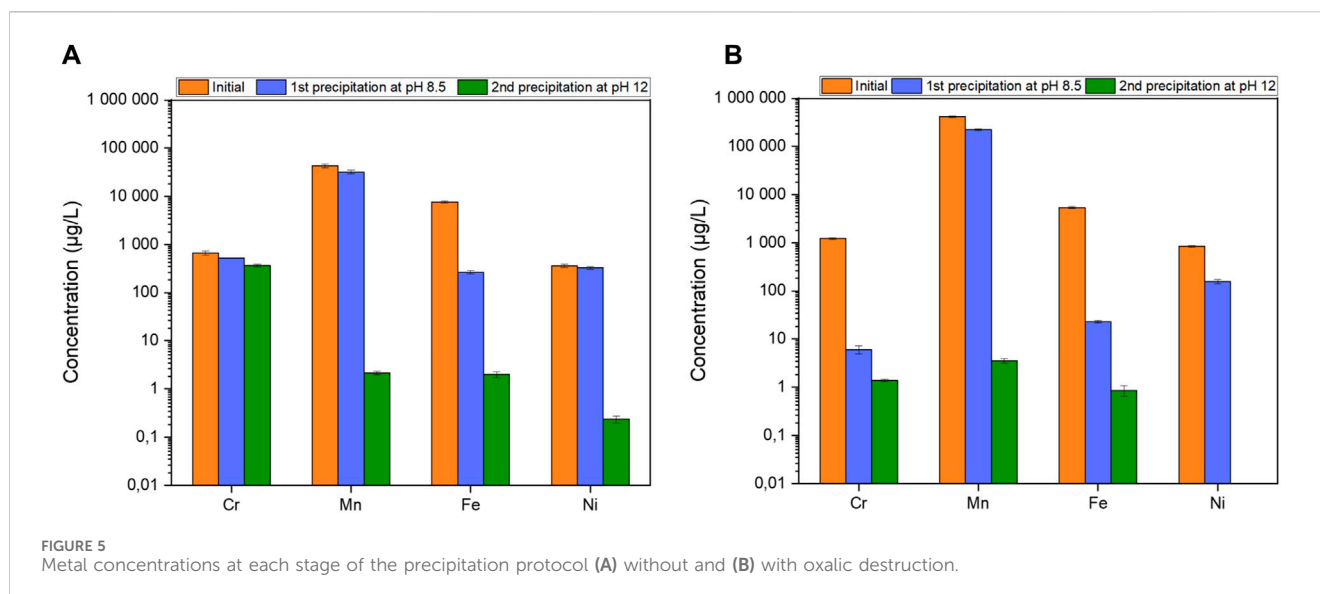
Although the total metal concentration was reduced by more than 29% (774 mg/L for 1 h compared with 288 mg/L for 24 h), a second precipitation is still required to eliminate Mn, Ni and Co. A visual evolution of the solution can be seen in Supplementary Data S1 in Supplementary Figure S1. The solution darkens over time and becomes completely black after 24 h of stirring.

One hypothesis is that the solution, being in contact with ambient oxygen, oxidizes over time, slowly precipitating Mn<sup>2+</sup> into black MnO<sub>2</sub>, which would explain the drop in Mn concentration between 8 and 24 h in Figure 4. This phenomenon was also observed by Wollast et al. (1979) with the oxidation of Mn<sup>2+</sup> in natural waters.

With a view to reduce environmental impact and handling costs, a LCA/LCC (Life Cycle Assessment/Life Cycle Costing) study has been carried out on this protocol by Clayton (2023) to evaluate the key parameters. It appears that the energy supplied during the protocol is the major contributor to the total environmental impact for a laboratory scale protocol. The contact time during the first precipitation was kept to 1 h to reduce energy demand as increased time of contact showed no significant improvements.

### 3.2.2 Effect of oxalic destruction

The results of the precipitation protocol applied to effluents G1 from the COREMIX process can be seen in Figure 5A. The concentrations of the four metals (Cr, Mn, Fe and Ni) present in the initial solution were measured at each stage of the precipitation protocol without prior destruction of the oxalic acid. The results show that Mn, Fe and Ni are removed from the solution at the end of the protocol with an efficiency of 100% ± 12%, 100% ± 8% and 100% ± 7%, respectively. Furthermore, the first precipitation seems to be effective for Fe, while the second is effective for Mn and Ni. However, with only 49% ± 6% precipitated at the end of the protocol, chromium did not behave in the same way as in the tests on synthetic samples in the work of Rivonkar et al. (2022). The results highlight the impact of oxalic acid on chromium



precipitation, but also show that it does not interfere with the precipitation of Mn, Fe and Ni. Two hypotheses have been investigated. The first one is based on the chemical form of chromium. It has two stable oxidation states in solution (+III and +VI). Depending on the pH of the solution, Cr(VI) can be found in the form of  $\text{HCrO}_4^-$  (acidic medium) or  $\text{CrO}_4^{2-}$  (alkaline medium) (Zhang and Tian, 2020).

As these compounds are soluble in aqueous media, this could explain the decrease in solid chromium in the precipitate in the form of  $\text{Cr}(\text{OH})_3$ . However, the oxalic acid present in the solution is a reducing agent for Cr(VI), transforming it into Cr(III) (Peng and Guo, 2020) and allowing precipitation. The second hypothesis therefore focuses on the interaction between chromium and oxalic acid. Oxalic acid can form stable and soluble  $\text{Cr}(\text{C}_2\text{O}_4)$  by reaction with chromium (II) in solution or by dissolution of chromium oxides and hydroxides, as seen in an US patent (Banda et al., 2009) and described by García Rodenas et al. (1997).

This interaction between oxalate and Cr competes with the formation of stable chromium hydroxide,  $\text{Cr}(\text{OH})_3$ , preventing its removal through filtration. According to Remoundaki et al. (2007), the higher the concentration of oxalate in solution, the higher the solubility of chromium. This is confirmed in Figure 5B, representing the effluent G2 which was also generated by the COREMIX process. The oxalic acid present in this sample was completely destroyed beforehand by the addition of  $\text{H}_2\text{O}_2$  at 80 °C for 48 h. In contrast to Figure 5A, 100% ± 6% of the chromium is removed. This confirms the need of an intermediate step for the destruction or removal of oxalic acid, prior to raising the pH of the solution for precipitation. This step although critical, uses significant amounts of energy required to heat for 48 h. This has a significant environmental impact at this scale, as seen in the LCA/LCC analysis by Clayton (Clayton (2023)). The author shows that this impact could vary based on country of implementation, depending on the origins of the energy source, i.e., the environmental impact of a country that produces its electricity from burning coal will be greater than that of a country that produces its electricity from renewable or nuclear sources.

### 3.2.3 Effect of precipitant

Two precipitants, NaOH and KOH, were tested on surrogate effluent (respectively G2 and G3) after destruction of the oxalic acid. The concentration of metals in solution (Cr, Mn, Fe and Ni) was measured for each sample after each precipitation. The percentage removal of each metal is summarized in Table 4.

The results show slight variations in precipitation efficiency at pH 8.5. The precipitation percentages are identical between the use of KOH and NaOH for elements with low solubility at pH 8.5, with 100% for chromium and iron. However, it appears that slightly more manganese and nickel were removed from the solution when NaOH was used, with 46% ± 6% of Mn and 82% ± 6% of Ni in the precipitate compared to 37% ± 6% of Mn and 71% ± 4% of Ni when KOH was used.

With regard to the second precipitation and, more generally, the total precipitation yield, the results show that the use of NaOH or KOH produces identical precipitation yields, with 100% for Cr, Mn, Fe and Ni. These results are in agreement with Kursunoglu and Kaya (2013) who report similar manganese precipitation efficiencies between NaOH and KOH with respectively 94% and 96% of Mn precipitated at pH 10.

As the overall yields are identical, either precipitant can be used to treat a solution containing metal ions. There are still some differences to be considered when applying the process on an industrial scale, such as the cost of reagents and specific storage conditions because of the carbonation of these compounds by atmospheric  $\text{CO}_2$  (Jagannathan et al., 2021). Moreover, the effect of natural  $^{40}\text{K}$  (0.0117%), which may require radiological precautions in large quantities, must also be taken into account.

## 3.3 Implementation on radioactive samples

### 3.3.1 COREMIX process

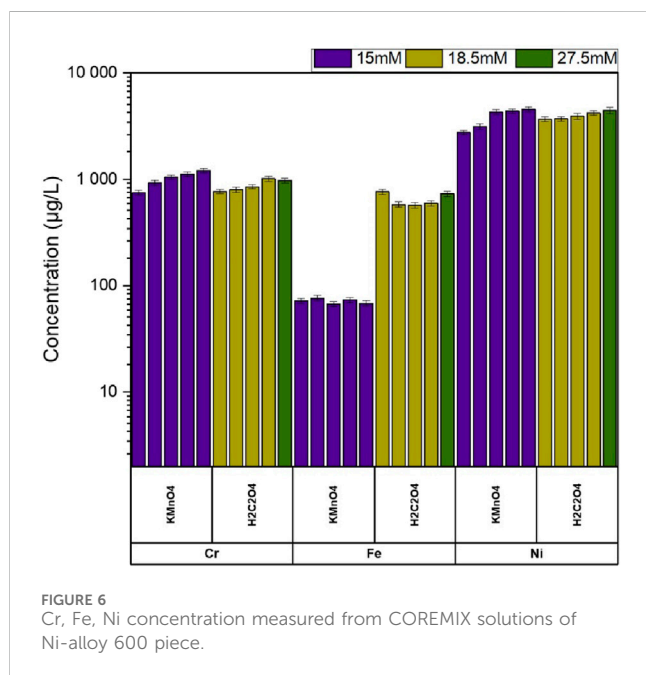
#### 3.3.1.1 Metallic dissolution efficiency

The optimized COREMIX protocol was implemented on radioactive sample M1, resulting in significant metal dissolution

TABLE 4 Removal efficiency of metals after each precipitation stage using KOH vs. NaOH.

	% Of precipitation							
	Cr		Mn		Fe		Ni	
	NaOH	KOH	NaOH	KOH	NaOH	KOH	NaOH	KOH
pH 8.5	100 ± 6	100 ± 5	46 ± 6	37 ± 6	100 ± 6	100 ± 7	82 ± 6	71 ± 4
pH 12	100 ± 6	100 ± 5	100 ± 7	100 ± 7	100 ± 6	100 ± 7	100*	100 ± 5

\*Concentration below quantification limit of ICP-MS, for Ni (0.1 µg/L).



as seen in Figure 6. Across the five cycles, the average dissolution values were found to be  $920 \pm 50$  µg/L for Cr,  $680 \pm 40$  µg/L for Fe, and  $4,160 \pm 240$  µg/L for Ni. Specifically, the first four cycles exhibited an average dissolution of  $860 \pm 40$  µg/L for Cr,  $630 \pm 40$  µg/L for Fe, and  $3880 \pm 210$  µg/L for Ni. Notably, the fifth cycle, employing a 50% higher concentration of oxalic acid, led to an increase of 12%–14% in the dissolution of Cr, Fe, and Ni compared to the average dissolution observed in the first four cycles.

The selectivity of potassium permanganate towards the dissolution of chromium oxide is clearly demonstrated in Figure 6, with minimal additional dissolution observed during the oxalic acid stage. The presence of  $\text{Cr}_2\text{NiO}_4$  oxide on such samples as found in the works of Machet (2004), McGrady (2017), leads to the simultaneous dissolution of nickel alongside chromium. Additionally, the preference for iron dissolution by oxalic acid is evident. These findings validate the necessity of an oxidative step in the COREMIX process to remove Cr-Ni oxides, as reported in the literature, and a reductive step involving oxalic acid for Fe-Ni oxides (Rivonkar et al., 2022; Ocken, 1999; Balaji et al., 2018; Wille and Bertholdt, 1998).

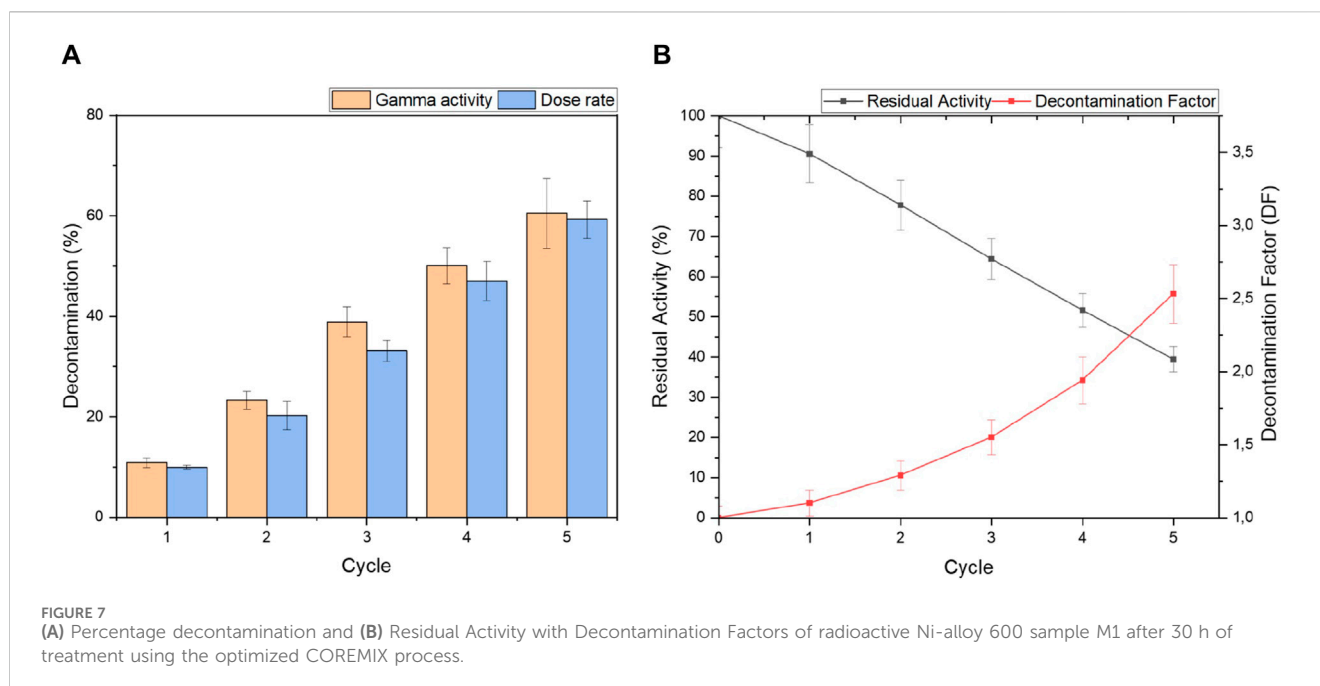
This was further emphasized when the process was identically applied on sample M2, except for the fifth cycle, wherein the time of contact was doubled to 6 h per step. For sample M2, the increased

contact time led to a 25% increase in Cr dissolution and a 19% increase in Ni dissolution whereas Fe dissolution was not significantly different, as presented in Supplementary Figure S2 in the Supplementary Data S1. This increase in Cr and Ni dissolution can be explained by the increased dissolution of Cr and Ni enriched oxides such as  $\text{Cr}_2\text{NiO}_4$ , which acts as a passive layer protecting the oxide.

A hypothesis can be formulated to explain the absence of a rise in iron dissolution with prolonged contact time. According to the properties of Ni-alloy 600, the high Ni and Cr content (72% and 14% compared to 6% for Fe) are responsible for the corrosion resistance of metal. The Ni also provides excellent corrosion resistance in the presence of reducing environment, which is the case during the oxalic acid stage (Newman, 2002). Machet and Voyshtnis showed in their respective works  $\text{Cr}_2\text{NiO}_4$  grows rapidly on the surface of the Ni-alloy 600 albeit upon exposure to high temperatures (350 °C). The authors noticed 1 nm of oxide being formed within 1 min of exposure, that is just over 40% of the total thickness of oxide formed after 100 h of exposure. 70% of this oxide thickness is the inner oxide consisting of mainly  $\text{Cr}_2\text{NiO}_4$  (Machet et al., 2007; Voyshtnis et al., 2018). Machet et al. (2007) suggested that in the early stages of oxidation (0.4–4 min), an ultra-thin layer (~1 nm) of chromium oxide ( $\text{Cr}_2\text{O}_3$ ) with an outer layer of  $\text{Cr}(\text{OH})_3$  and  $\text{Ni}(\text{OH})_2$  forms on the surface. After 4–8 min, both an inner layer ( $\text{Cr}_2\text{O}_3$ ) and outer layer of  $\text{Ni}(\text{OH})_2$  thicken on the surface.

Due to this corrosion resistance nature of the Ni-alloy-600, the protective  $\text{Cr}_2\text{NiO}_4$  is formed during the treatment process with oxalic acid, most likely at a slower pace due to the reduced temperature as compared to the works of Machet and Voyshtnis. This layer is also insoluble once the permanganate ion ( $\text{MnO}_4^-$ ) has been reduced. This implies that once a well-defined protective layer is established, oxalic acid is unable to continue dissolving the oxide layer and the underlying base metal surface. Any dissolution taking place by oxalic acid likely occurs during the initial stages before a protective film is completely formed. This could be the reason for the lack in increase in the dissolution of Fe after increased time of contact. However, it is important to note that since the entire sample was placed into the decontamination solution, the internal surface of the samples oxidized by primary circuit water, the cut edges of the samples and the external surface of the samples, oxidized by water of the secondary circuit, were all exposed to the solution, therefore potentially reducing the efficiency of the solution as compared to treatment of only the internal surface.

In order to compare the efficiency of the two processes (CORD and COREMIX), the mass loss corrosion rate was calculated for sample M2 according to Eq 1. With a mass loss of  $2.3 \pm 0.1$  mg, the



theoretical density of Ni-alloy 600,  $8.47 \text{ g/cm}^3$  and the surface area of the sample M2,  $134.3 \pm 0.6 \text{ mm}^2$  the mass loss corrosion rate is equal to  $0.056 \pm 0.002 \text{ } \mu\text{m/h}$ . The corrosion rate of alloy 600 in the optimized COREMIX process is twice as high compared to the corrosion rate reported by Jung et al. (2015). In their study, the authors observed a corrosion rate of approximately  $0.025 \text{ } \mu\text{m/h}$  ( $0.001 \text{ mil/h}$ ) in pure  $15.8 \text{ mM}$  oxalic acid at  $90^\circ\text{C}$ . This difference indicates that the optimized COREMIX process has significantly improved efficiency for Ni-alloy.

### 3.3.1.2 Metallic decontamination efficiency

Gamma spectrometry analysis was conducted on sample M1 at the beginning and at the end of each cycle. The counting conditions were kept identical for all cycles. After the fifth cycle, sample M1 was air-dried for a period of 4 days, resulting in a change in sample mass for the gamma spectrometry model. The initial characterization of the Ni-alloy 600 sample M1 show the presence of  $^{54}\text{Mn}$ ,  $^{57}\text{Co}$ ,  $^{60}\text{Co}$  and  $^{125}\text{Sb}$  (Table 1) with a total activity of  $13,920 \pm 790 \text{ Bq}$  detected, with over 99% coming from  $^{60}\text{Co}$ .

The decontamination factor, representing the efficiency of the COREMIX process, remained constant with an average value of  $12\% \pm 2\%$  per cycle as seen in Figure 7A. The percentage of total decontamination between the initial activity and activity after cycle five reached  $60\% \pm 7\%$ , indicating a substantial reduction in activity in 30 h of treatment. The factor was calculated as  $2.5 \pm 0.2$ , highlighting the degree of decontamination achieved after five cycles.

The residual activity remaining in the sample, as depicted in Figures 7B, 7is at  $39\% \pm 3\%$ . Based on the average decontamination rate of  $12\% \pm 2\%$  per cycle, an additional 3-4 cycles would be required to eliminate this remaining activity assuming linear decontamination behaviour for each cycle. The additional cycles were not performed to limit the dose exposure of the workers as the dose characterization necessitates near-direct contact with the sample of this geometry.

The dose evolution of the sample M1 is presented in Table 5. The decontamination factors after each cycle were coherent with those obtained using gamma spectrometry.

## 3.3.2 Precipitation process

### 3.3.2.1 Effluent precipitation efficiency

As the precipitation protocol is feasible for surrogate liquid samples, it was applied to the effluent R1 and R2 from the contaminated Ni-alloy 600 sample M1 and M2 treated using the COREMIX process. The results in Figure 8 present Cr, Mn, Fe and Ni concentrations measured after the COREMIX-H process (initial sample), after the first precipitation (pH 8.5) and after the second precipitation (pH 12).

The results obtained are in line with those found on the G2 and G3 surrogate samples. This correlation proves that the type of metal being decontaminated does not affect the precipitation protocol, which works for both 316Ti stainless steel and Ni alloy samples. These data highlight also the importance of carrying out two separate precipitations.

The first precipitation at pH 8.5 led to a decrease of  $91\% \pm 3\%$  in Cr,  $20\% \pm 6\%$  in Mn,  $93\% \pm 7\%$  in Fe and  $25\% \pm 7\%$  in Ni. These values are slightly lower than those found by Fu and Wang (2011), Yatim et al. (2021) for chromium, with respective removal efficiencies of 100% at pH 8.7 and pH 10.

This observation can also be made for iron with the results of Oncel et al. (2013), Balintova and Petrilakova (2011) who found that 100% and 97% of iron was precipitated around pH 8. These authors, in addition, state that 16% of manganese is removed at a pH of 8.2, a value close to that found previously. Although the values remain in the same order of magnitude, different working matrices, pH and metal concentrations can explain these slight differences between all the results.

After the second precipitation at pH 12,  $99\% \pm 1\%$  of Cr and  $100\% \pm 7\%$  of Mn were removed from the solution, as well as  $99\% \pm 7\%$  of Fe and  $100\% \pm 8\%$  of Ni. Figure 8 clearly demonstrates the

TABLE 5 Dose evolution of radioactive Ni-alloy 600 sample M1 throughout the process using different detectors.

Sample	Stage	Colibri (μSv/h)	AD-6 (μSv/h)	Gamma probe (cps)	X-ray probe (cps)
Metallic Sample	Initial	8	25	1,640	770
	After 1st cycle	9	22	1,520	710
	After 2nd cycle	8	16	1,290	600
	After 3rd cycle	6	15	1,120	500
	After 4th cycle	5	11	890	390
	After 5th cycle <sup>a</sup>	4	8	700	310
Effluent <sup>b</sup>	Initial <sup>c</sup>	160	0	40	6
	After 1st precipitation	110	1	25	15
	After 2nd precipitation	3	0	2	0
Sludge <sup>d</sup>	1st precipitate	104	1	23	8
	2nd precipitate	2,960	6	497	190

All values taken after stabilization of signal and adjusted for background.

<sup>a</sup>Cycle 5 with 50% higher oxalic acid.

<sup>b</sup>Dose evaluation of liquids done using 50 mL aliquot in HDPE, tubes used for gamma spectrometry; measured from the bottom.

<sup>c</sup>Measured after oxalic acid destruction stage.

<sup>d</sup>Measured by placing filter paper inside Petri dish, without drying.

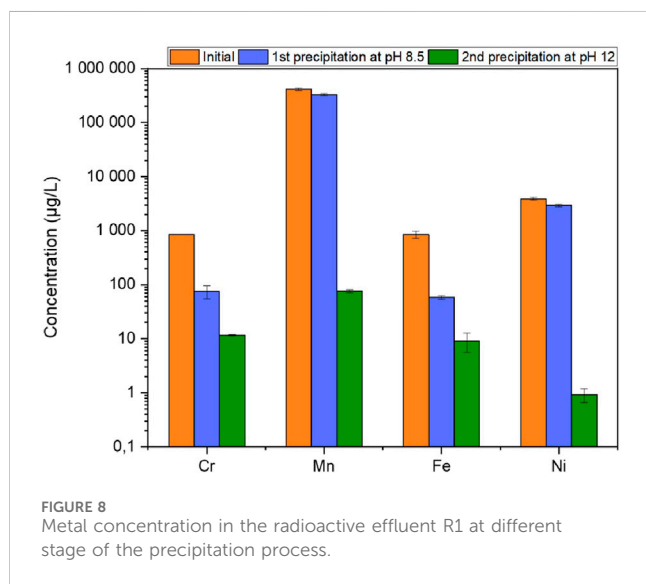


FIGURE 8 Metal concentration in the radioactive effluent R1 at different stage of the precipitation process.

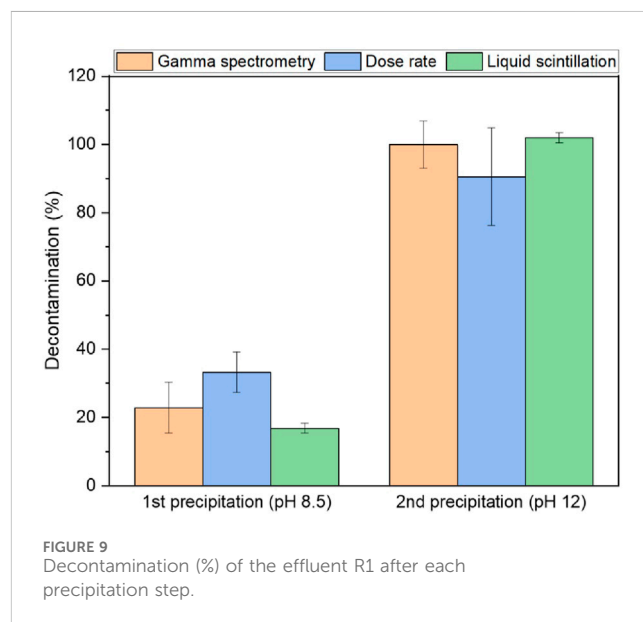


FIGURE 9 Decontamination (%) of the effluent R1 after each precipitation step.

benefits of raising the pH to 12 to precipitate Ni and Mn. This observation was also made by Balintova and Petrilakova (2011), showing that an increase in pH precipitates 90% of Mn at pH 10. Ni was removed from the solution and precipitated quantitatively, as demonstrated in the study carried out by Tsai et al. (2020) with around 100% of removal at pH 12. Liu et al. (2020) found similar results with 100% of Ni in the solid after precipitation at pH 10 and 11. Similar results were found when the radioactive sample R2 treated by the same process was analyzed. The concentration results are presented in Supplementary Figure S3 in the Supplementary Data S1.

The stable isotope <sup>59</sup>Co was also measured by ICP-MS but its concentration was below the quantification limits (0.1 μg/L in <sup>59</sup>Co) after accounting for the dilution procedures to limit the total

radioactivity level (< 1 Bq) and prevent instrument contamination (internal radioprotection procedure).

### 3.3.2.2 Decontamination efficiency of effluent

As cobalt is present in trace amounts, its precipitation yield is tracked by its activity in solution after each precipitation. The efficiency of radioactive effluent decontamination was measured using gamma spectrometry, liquid scintillation and dose rate measurements. All the results are shown in Figure 9 and details of dose rate measurements are shown in Table 5.

At pH 8.5, the radioactivity present in the radioactive effluent appears to have decreased by 24% ± 10% (average calculated using

TABLE 6 Gamma spectrometry results of the precipitation process for each radionuclide in solution and calculation of the associated decontamination factor.

Radionuclides	Initial specific radioactivity (Bq/L)	Final specific radioactivity (Bq/L)	Decontamination factor
<sup>54</sup> Mn	90 ± 14	≤ 1.4*	≥ 63
<sup>60</sup> Co	15,800 ± 800	5 ± 1	3290 ± 560
<sup>125</sup> Sb	80 ± 30	≤ 4.5*	≥ 19

\*Activity below detection limit of gamma spectrometer for <sup>54</sup>Mn and <sup>125</sup>Sb respectively.

the three techniques). However, when the pH reached 12, 98% ± 16% of the radioactivity appears to be eliminated with the removal of the main radioactive emitters present in solution <sup>54</sup>Mn, <sup>60</sup>Co and <sup>125</sup>Sb (Table 1). According to Inam et al. (2019), around 90% of Sb is expected to precipitate at pH 8.5, while more alkaline conditions are required to remove Mn as seen earlier. As the activity of these two radionuclides (<sup>54</sup>Mn and <sup>125</sup>Sb) is very low, it is the behavior of <sup>60</sup>Co that has the greatest impact on the decontamination factor. The minimum solubility of Co (II) in the presence of hydroxide ions is at pH 11 where it precipitates as Co(OH)<sub>2</sub> as showed by Gaudaire J M (1999). This is experimentally confirmed by Oh et al. (2023) finding that 99.4% of Co is removed from the solution between pH 10 and 12. These data prove that the significant decontamination factor at pH 12 is consistent, but this does not explain why 24% of the activity of the initial solution is removed during the first precipitation pH 8.5. To understand this, the behavior of cobalt must be studied taking into account the other elements present in the solution.

According to Lehto and Hou (2010), Co can be precipitated at a lower pH value in the presence of a carrier and iron hydroxide Fe(OH)<sub>3</sub> which is the main compound of the solid generated at pH 8.5 co-precipitates metals effectively by adsorption. This explain why some of the cobalt is precipitated during the first pH adjustment, leading to a 24% reduction in radioactivity.

The initial and final activity of the various radionuclides in solution R1 are shown in Table 6 as well as their associated decontamination factor. At the end of the hydroxide precipitation protocol, the decontamination factor is at least 63 for <sup>54</sup>Mn, at least 19 for <sup>125</sup>Sb (as their activities are too low, the detection limit of the device is considered) and 3290 ± 560 for <sup>60</sup>Co. Finally, the total decontamination factor (which includes all the radionuclides) of the contaminated effluent R1 is 3330 ± 560. The decontamination factor of the active sample R2 is shown in Supplementary Figure S4 in Supplementary Data S1. This liquid effluent was decontaminated by the same precipitation process as sample R2 and shows a total decontamination factor of 5,810 ± 410.

Measurement of beta emitters like <sup>55</sup>Fe, <sup>63</sup>Ni, <sup>90</sup>Sr and <sup>99</sup>Tc, if present, is planned in order to quantify them and study their behavior during the entire decontamination protocol (including COREMIX process, oxalic acid destruction and precipitation).

## 4 Conclusion

In this study, the process of precipitating metals in the form of hydroxides as part of the decontamination of effluents

generated by the COREMIX process was investigated. Tests were carried out on synthetic, surrogate and radioactive samples to assess the efficiency of the protocol. The precipitation protocol was first optimized and then the solid compounds produced were characterized to determine their composition and chemical form. Finally, the COREMIX-HP process was applied to real radioactive Ni-alloy 600 samples to measure the decontamination factors of each process.

The various solids characterization methods (FTIR, XRD and TGA-DSC) showed that the sludge produced at pH 8.5 during the precipitation process is mainly composed of iron oxide-hydroxide, while the sludge formed during the second step, at pH 12, is composed of manganese oxide Mn<sub>3</sub>O<sub>4</sub>. The influence of the contact time during the first precipitation and of the type of reagent used has been studied and it appears that their effects are insignificant. The use of either KOH or NaOH seems to lead to almost total precipitation of metals in solution. Furthermore, it has been observed that samples treated by the COREMIX process need to be pre-treated before precipitation. Indeed, the oxalic acid contained in the effluents prevents the efficient precipitation of chromium leading to only 49% of removal instead of 100%, so a heating step with the addition of H<sub>2</sub>O<sub>2</sub> is necessary to destroy oxalic acid.

The efficiency of the previously optimized COREMIX process was reproduced onto real radioactive Ni-alloy 600 samples with about 60%–70% decontamination achieved in 30 h of treatment. In addition, it appears that the efficiency of the COREMIX process has improved compared to the CORD process based on the mass loss corrosion rate results. Then, it was seen that the inherit corrosion resistance property of Ni-alloy 600 hinders the process over time, as the corrosion resistance by forming of a barrier oxide layer, reduces the efficiency of oxalic acid as contact time is increased. This suggests the need of using shorter cycle times, with 3 h being sufficient per cycle step, as anything beyond was seen to have insignificant contribution. This configuration allows for 12%–14% decontamination per cycle of the process, suggesting a total of 8–9 cycles required for complete decontamination. The effluents generated during the COREMIX process were collected in order to test the efficiency of the precipitation protocol on active samples. It was observed that the first precipitation stage carried out at pH 8.5 was not sufficient to decontaminate the effluents, with only a 24% drop in total radioactivity. However, the second precipitation step remarkably improved the decontamination factor to several thousands, making the protocol almost 100% effective.

Further optimization can be done on the scale-up of the COREMIX-HP process from the current batch process to a more

dynamic process to better simulate decontamination of a Ni-alloy 600 steam generator in nuclear power plants, where the flow rate of the solution could play an important role. Further optimization is also required for the effluent treatment stages. The heating time required to destroy the oxalic acid still needs to be refined in order to reduce the energy costs associated with this stage. As for the precipitation process, different types of precipitants, such as sulfides, phosphates and electrocoagulation, could be studied in order to be able to adapt the protocol to effluents from different materials or decontamination processes. The various metals present in the effluent continue to remain in trace quantities after the precipitation protocol. Therefore, a chromatographic resin purification step must be developed and optimized to meet radioactive waste acceptance criteria and to be able to treat the final effluent as conventional waste. Finally, scaling up the COREMIX-HP process will lead to a significant increase in the amount of waste generated. Therefore, scale-up trials must also be carried out on the precipitation stages to ensure that it is effective on an industrial scale.

## Data availability statement

The raw data supporting the conclusions of this article will be made available by the authors, without undue reservation.

## Author contributions

MR: Data curation, Formal Analysis, Investigation, Methodology, Validation, Visualization, Writing—original draft, Writing—review and editing. AR: Data curation, Formal Analysis, Investigation, Methodology, Writing—original draft, Writing—review and editing. TS-M: Methodology, Supervision, Validation, Writing—review and editing. AA: Conceptualization, Funding acquisition, Project administration, Supervision, Validation, Writing—review and editing. MM: Methodology, Supervision, Validation, Writing—review and editing.

## References

- Atique Ullah, A. K. M., Fazle Kibria, A. K. M., Akter, M., Khan, M. N. I., Tareq, A. R. M., and Firoz, S. H. (2017). Oxidative degradation of methylene blue using  $Mn_3O_4$  nanoparticles. *Water Conservation Sci. Eng.* 1, 249–256. doi:10.1007/s41101-017-0017-3
- Baja, B., Varga, K., Szabó, N. A., Németh, Z., Kádár, P., Oravetz, D., et al. (2009). Long-term trends in the corrosion state and surface properties of the stainless steel tubes of steam generators decontaminated chemically in VVER-type nuclear reactors. *Corros. Sci.* 51, 2831–2839. doi:10.1016/j.corsci.2009.08.007
- Balaji, V., Chandramohan, P., Rangarajan, S., and Velmurugan, S. (2018). Dissolution of nickel and chromium from Ni-Cr-Fe-O oxide by oxidative treatment with permanganate. *Prog. Nucl. Energy* 104, 136–142. doi:10.1016/j.pnucene.2017.09.008
- Balek, V., and Subrt, J. (1995). Thermal behaviour of iron(III) oxide hydroxides. *Pure Appl. Chem.* 67, 1839–1842. doi:10.1351/pac199567111839
- Balintova, M., and Petrilakova, A. (2011). Study of pH influence on selective precipitation of heavy metals from acid mine drainage. *Chem. Eng. Trans.* 25, 345–350. doi:10.3303/CET1125058
- Banda, T., Koike, S., and Hara, T. (2009). Organic acid chromium (iii) salt aqueous solution and process of producing the same. Available at: <https://patents.google.com/patent/US20090194001A1/en>.US20090194001A1 (Accessed August 10, 2023).
- Bertolucci, E., Galletti, A., Antonetti, C., Marracci, M., Tellini, B., Piccinelli, F., et al. (2015). "Chemical and magnetic properties characterization of magnetic nanoparticles," in Conference Record - IEEE Instrumentation and Measurement Technology Conference 2015, Pisa, Italy, 11-14 May 2015, 1492–1496.
- Blenkinsop, J., Rivonkar, A., Robin, M., Carey, T., Dunnett, B., Suzuki-Muresan, T., et al. (2024). Methods for the destruction of oxalic acid decontamination effluents (accepted on 16 february 2024). *Front. Nucl. Eng.* 1. doi:10.3389/fnuen.2024.1347322
- Chouchaine, A., Marzouk-Trifi, I., Trifi, B., Ghodbane, O., Dhaouadi, H., Touati, F., et al. (2022). Synthesis, characterization of  $Mn_3O_4$ : adsorption application and antibacterial evaluation. *J. Chil. Chem. Soc.* 67, 5582–5586. doi:10.4067/S0717-97072022000305582
- Clayton, R. (2023). Approaches to LCA in WP4 and WP7, (PREDIS Life cycle analysis and - costing webinar). Available at: <https://predis-h2020.eu/life-cycle-analysis-and-costing-webinar/>.
- Cornell, R. M., Giovanoli, R., and Schneider, W. (1989). Review of the hydrolysis of iron(III) and the crystallization of amorphous iron(III) hydroxide hydrate. *J. Chem. Technol. Biotechnol.* 46, 115–134. doi:10.1002/jctb.280460204280460204
- Cravotta, C. A. (2008). Dissolved metals and associated constituents in abandoned coal-mine discharges, Pennsylvania, USA. Part 2: geochemical controls on constituent concentrations. *Appl. Geochem.* 23, 203–226. doi:10.1016/j.apgeochem.2007.10.003
- Daou, T. J. (2007). "Synthèse et fonctionnalisation de nanoparticules d'oxydes de fer magnétiques," (Strasbourg: Université Louis Pasteur), 1971–2008. Ph.D Thesis.

## Funding

The author(s) declare that financial support was received for the research, authorship, and/or publication of this article. This work was carried out under the PREDIS European project. This project has received funding from the European Union's Horizon 2020 research and innovation programme under agreement No. 945098.

## Acknowledgments

We would like to thank Eric Chevrel, technician in the Energy Systems and Environment Department at IMT Atlantique for his help and advice during the TGA analyses.

## Conflict of interest

The authors declare that the research was conducted in the absence of any commercial or financial relationships that could be construed as a potential conflict of interest.

## Publisher's note

All claims expressed in this article are solely those of the authors and do not necessarily represent those of their affiliated organizations, or those of the publisher, the editors and the reviewers. Any product that may be evaluated in this article, or claim that may be made by its manufacturer, is not guaranteed or endorsed by the publisher.

## Supplementary material

The Supplementary Material for this article can be found online at: <https://www.frontiersin.org/articles/10.3389/fnuen.2024.1396821/full#supplementary-material>

- Demmer, R. (1994). Testing and evaluation of eight decontamination chemicals. WINCO-1228. United States: WestingHouse Idaho Nuclear Company, Inc.
- Deng, D., Zhang, L., Dong, M., Samuel, R. E., Ofori-Boadu, A., and Lamssali, M. (2020). Radioactive waste: a review. *Water Environ. Res.* 92, 1818–1825. doi:10.1002/wer.1442
- Durmuz, Z., Kavas, H., Baykal, A., and Toprak, M. S. (2009). A green chemical route for the synthesis of Mn3O4 nanoparticles. *Central Eur. J. Chem.* 7, 555–559. doi:10.2478/s11532-009-0049-4
- Ellen MacArthur Foundation (2020). How to build a circular economy. Available at: <https://ellenmacarthurfoundation.org/> (Accessed on July 28, 2023).
- EURAD (2020). Current use of waste acceptance criteria (WAC) in European union member-states and some associated countries. Milestone 88, EJP EURAD. Available at: <https://www.ejp-eurad.eu/publications/eurad-milestone-88-current-use-waste-acceptance-criteria-european-union-members-states> (Accessed on August 17, 2023).
- European Commission (2014). *Life-cycle costing*. Available at: <https://green-business.ec.europa.eu/green-public-procurement/life-cycle-costing> (Accessed on August 18, 2023).
- European Commission (2016). *Nuclear illustrative programme, ref: com(2016)177*. Official Journal of the European Union, 104–110.
- Fu, F., and Wang, Q. (2011). Removal of heavy metal ions from wastewaters: a review. *J. Environ. Manag.* 92, 407–418. doi:10.1016/j.jenvman.2010.11.011
- García Rodenas, L. A., Iglesias, A. M., Weisz, A. D., Morando, P. J., and Blesa, M. A. (1997). Surface complexation description of the dissolution of chromium(III) hydroxous oxides by oxalic acid. *Inorg. Chem.* 36, 6423–6430. doi:10.1021/ic9709382
- Gaudaire, J. M. (1999). "Etude de la spéciation du 60Co dans les effluents de l'usine de retraitement de combustibles irradiés de la Hague; devenir après rejet dans les eaux de la Manche," (Orsay: Université Paris Sud). Ph.D. thesis.
- Geissdoerfer, M., Pieroni, M. P., Pigosso, D. C., and Soufani, K. (2020). Circular business models: a review. *J. Clean. Prod.* 277, 123741. doi:10.1016/j.jclepro.2020.123741
- Giorgi, S., Lavagna, M., and Campioli, A. (2019). Lca and lcc as decision-making tools for a sustainable circular building process. *IOP Conf. Ser. Earth Environ. Sci.* 296, 012027. doi:10.1088/1755-1315/296/1/012027
- Guidi, G., Cumo, F., and De Santoli, L. (2010). LCA of strippable coatings and steam vacuum technology used for nuclear plants decontamination. *Clean Technol. Environ. Policy* 12, 283–289. doi:10.1007/s10098-009-0208-5
- W. M. Haynes (2006). *CRC handbook of chemistry and physics: a ready-reference book of chemical and physical data*. 2007 edn (Boca Raton, Fla: CRC, Taylor & Francis), 87.
- Hirose, R., and McCauley, D. (2022). The risks and impacts of nuclear decommissioning: stakeholder reflections on the UK nuclear industry. *Energy Policy* 164, 112862. doi:10.1016/j.enpol.2022.112862
- Hu, Y., Long, X., Dong, L., Tan, Z., Tang, W., and Huang, Z. (2018). A decontamination technique for the primary cooling circuit of the research type nuclear reactor. *Nucl. Eng. Des.* 337, 318–323. doi:10.1016/j.nucengdes.2018.07.019
- IAEA (1983). *Characteristics of radioactive waste forms Conditioned for Storage and disposal: Guidance for the Development of waste acceptance criteria*. International Atomic Energy Agency.
- IAEA (1992). *Chemical precipitation processes for the treatment of aqueous radioactive waste*. Vienna: International Atomic Energy Agency, 337.
- Inam, M. A., Khan, R., Akram, M., Khan, S., and Yeom, I. T. (2019). Effect of water Chemistry on antimony removal by chemical coagulation: implications of  $\zeta$ -potential and size of precipitates. *Int. J. Mol. Sci.* 20, 2945. doi:10.3390/ijms20122945
- Jagannathan, T., Chandramouli, A., Ramachandran, K., Dev, S., Devi, E. L., Sharma, K., et al. (2021). Use of drone with sodium hydroxide carriers to absorb carbon dioxide from ambient air. *J. Emerg. Investigators* 4, 5. doi:10.59720/21-006
- Jung, J. Y., Park, S. Y., Won, H. J., Kim, S. B., Choi, W. K., Moon, J. K., et al. (2015). Corrosion properties of Inconel-600 and 304 stainless steel in new oxidative and reductive decontamination reagent. *Metals Mater. Int.* 21, 678–685. doi:10.1007/s12540-015-4572-x
- Kursunoglu, S., and Kaya, M. (2013). Dissolution and precipitation of zinc and manganese obtained from spent zinc-carbon and alkaline battery powder. *Fizykochemiczne Problemy Mineralurgii - Physicochem. Problems Mineral Process.* 50. doi:10.5277/ppmp140104
- Kutz, M. (2005). *Handbook of environmental degradation of materials*. 2 edn. Elsevier: William Andrew Publishing.
- Laversin, H. (2006). "Traceurs et formes chimiques du fer dans les particules émises dans l'atmosphère depuis un site sidérurgique: Etude spectroscopique et caractérisation de composés de référence et de particules collectées dans l'environnement," (Université du Littoral - Côte d'Opale). Ph.D. Thesis.
- Lehto, J., and Hou, X. (2010). *Chemistry and analysis of radionuclides*. John Wiley & Sons. doi:10.1002/9783527632770
- Leontie, L., Doroftei, C., and Carlescu, A. (2018). Nanocrystalline iron manganite prepared by sol-gel self-combustion method for sensor applications. *Appl. Phys. A* 124, 750. doi:10.1007/s00339-018-2175-3
- Liu, Y., Ding, W., Zhang, Y., Shen, F., Yang, G., He, Y., et al. (2020). A comparative study of nickel(II) removal from electroplating wastewater by pre-precipitation combined with Fenton-precipitation or Fenton-like-precipitation. *Desalination Water Treat.* 182, 220–224. doi:10.5004/dwt.2020.25223
- Machet, A. (2004). Study of the initial stages of oxidation of stainless steels in high temperature water. *Chem. Chim. ParisTech* 235. Ph.D Thesis.
- Machet, A., Galtayries, A., Marcus, P., Jolivet, P., Foucault, M., Combrade, P., et al. (2007). "Kinetics of passivation of a nickel-base alloy in high temperature water," in *Corrosion issues in light water reactors* (Elsevier), 44–56. doi:10.1533/9781845693466.1.44
- Malaret, F., and Yang, X.-S. (2022). Exact calculation of corrosion rates by the weight-loss method. *Exp. Results* 3, e13. doi:10.1017/exp.2022.5
- Mazo-Zuluaga, J., Barrero, C. A., Díaz-Terán, J., and Jerez, A. (2003). Thermally induced magnetite-haematite transformation. *Hyperfine Interact.* 148, 153–161. doi:10.1023/B:HYPE.0000003776.84005.89
- McGrady, J. (2017). "The effect of water Chemistry on corrosion product build-up under PWR primary coolant conditions," (University of Manchester). Ph.D. thesis.
- Mirion Technologies (2021). Colibri TTC & colibri VLD hand-held health physics communication. Available at: <https://www.mirion.com/products/technologies/health-physics-radiation-safety-instruments/portable-radiation-measurement/handheld-health-physics-instruments/colibri-ttc-colibri-vld-hand-held-health-physics-communication-alara-platform> (Accessed on April 15, 2023).
- Mishra, P. K., and Das, R. P. (1992). Kinetics of zinc and cobalt sulphide precipitation and its application in hydrometallurgical separation. *Hydrometallurgy* 28, 373–379. doi:10.1016/0304-386X(92)90042-X
- Muralikrishna, I. V., and Manickam, V. (2017). "Chapter five - Life cycle assessment," in *Environmental management*. Editors I. V. Muralikrishna and V. Manickam (Butterworth-Heinemann), 57–75. doi:10.1016/B978-0-12-811989-1.00005-1
- Mürbe, J., Rechtenbach, A., and Töpfer, J. (2008). Synthesis and physical characterization of magnetite nanoparticles for biomedical applications. *Mater. Chem. Phys.* 110, 426–433. doi:10.1016/j.matchemphys.2008.02.037
- Murray, A. (1986). A chemical decontamination process for decontaminating and decommissioning nuclear reactors. *Nucl. Technol.* 74, 324–332. doi:10.13182/NT86-A33835
- Nasrazadani, S. (1997). The application of infrared spectroscopy to a study of phosphoric and tannic acids interactions with magnetite (Fe3O4), goethite ( $\alpha$ -FeOOH) and lepidocrocite ( $\gamma$ -FeOOH). *Corros. Sci.* 39, 1845–1859. doi:10.1016/S0010-938X(97)00060-7
- Newman, I. (2002). The characteristics of INCONEL Alloy 600. Available at: <https://www.corrotherm.co.uk/blog/the-characteristics-of-inconel-alloy-600> (Accessed on June 19, 2023).
- Ocken, H. (1999). *Decontamination handbook*. Palo Alto, CA: EPRI, 112352.
- Oh, M., Lee, K., Jeon, M. K., Foster, R. I., and Lee, C.-H. (2023). Chemical precipitation-based treatment of acidic wastewater generated by chemical decontamination of radioactive concrete. *J. Environ. Chem. Eng.* 11, 110306. doi:10.1016/j.jece.2023.110306
- Oncel, M. S., Muhcu, A., Demirbas, E., and Kobya, M. (2013). A comparative study of chemical precipitation and electrocoagulation for treatment of coal acid drainage wastewater. *J. Environ. Chem. Eng.* 1, 989–995. doi:10.1016/j.jece.2013.08.008
- Peng, H., and Guo, J. (2020). Reduction behavior of chromium(VI) with oxalic acid in aqueous solution. *Sci. Rep.* 10, 17732. doi:10.1038/s41598-020-74928-7
- Perachiselvi, M., Bagavathy, S., Samraj, J., Pushpalaksmi, E., and Gurusamy, A. (2020). Synthesis and characterization of Mn3O4 nanoparticles for biological studies. *Appl. Ecol. Environ. Sci.* 8 (5), 273–277. doi:10.12691/aees-8-5-13
- Qi, D. (2018). "Chapter 6 - ion-exchange and extraction chromatography separation of rare earth elements," in *Hydrometallurgy of rare earths*. Editor D. Qi (Elsevier), 631–669. doi:10.1016/B978-0-12-813920-2.00006-4
- Radó, K., Varga, K., Németh, Z., Varga, I., Somlai, J., Oravetz, D., et al. (2004). A systematic study of the corrosion effects of the framatome CORD-UV technology. *Acad. Appl. Res. Mil. Sci.* 3, 171–175.
- Remoundaki, E., Hatzikioseyan, A., and Tsezos, M. (2007). A systematic study of chromium solubility in the presence of organic matter: consequences for the treatment of chromium-containing wastewater. *J. Chem. Technol. Biotechnol.* 82, 802–808. doi:10.1002/jctb.1742
- Rivonkar, A. (2023). "Optimization of chemical decontamination methods for radioactive metals," (Ecole nationale supérieure Mines-Télécom Atlantique Bretagne Pays de la Loire). Ph.D Thesis.
- Rivonkar, A., Katona, R., Robin, M., Suzuki-Muresan, T., Abdelouas, A., Mokili, M., et al. (2022). Optimisation of the chemical oxidation reduction process (CORD) on surrogate stainless steel in regards to its efficiency and secondary wastes. *Front. Nucl. Eng.* 1. doi:10.3389/fnuen.2022.1080954
- Saphymo (2015). Radiamètre portable Gamma et X Radioprotection portable Industrie Nucléaire. Available at: <http://www.saphymo.de/strahlungsmessung/radioprotection-portable/6150-ad5-6150-ad6/44.htm> (Accessed on April 15, 2023).

- Seehra, M. S., Roy, P., Raman, A., and Manivannan, A. (2004). Structural investigations of synthetic ferrihydrite nanoparticles doped with Si. *Solid State Commun.* 130, 597–601. doi:10.1016/j.ssc.2004.03.022
- Seifu, D., Kebede, A., Oliver, F. W., Hoffman, E., Hammond, E., Wynter, C., et al. (2000). Evidence of ferrimagnetic ordering in FeMnO<sub>3</sub> produced by mechanical alloying. *J. Magnetism Magnetic Mater.* 212, 178–182. doi:10.1016/S0304-8853(99)00787-8
- Shahadat, M., Rafatullah, M., and Teng, T. (2013). Characterization and sorption behavior of natural adsorbent for exclusion of chromium ions from industrial effluents. *Desalination Water Treat.* 53, 1–9. doi:10.1080/19443994.2013.855678
- Shelenkova, V., and Kulagina, T. (2021). Refinement of a decontamination technology for radioactively contaminated equipment. *Radioact. Waste* 14, 28–38. doi:10.25283/2587-9707-2021-1-28-38
- Special Metals (2008). Inconel alloy 600. Available at: <https://www.specialmetals.com/documents/technical-bulletins/inconel/> (Accessed on June 15, 2023).
- Sphera (2020). What is Life cycle assessment (LCA) ? Available at: <https://sphera.com/glossary/what-is-a-life-cycle-assessment-lca/> (Accessed on August 18, 2023).
- Taitel-Goldman, N. (2015). “Crystallization of Fe and Mn oxides-hydroxides in saline and hypersaline environments and *in vitro*,” in *Advanced topics in crystallization* (IntechOpen).
- Tian, Z., Song, L., and Li, X. (2019). Effect of oxidizing decontamination process on corrosion property of 304L stainless steel. *Int. J. Corros.* 2019, 1–6. doi:10.1155/2019/1206098
- Tsai, T.-H., Chou, H.-W., and Wu, Y.-F. (2020). Removal of nickel from chemical plating waste solution through precipitation and production of micro-sized nickel hydroxide particles. *Sep. Purif. Technol.* 251, 117315. doi:10.1016/j.seppur.2020.117315
- Valencia, L. (2012). “Radioactive waste management in nuclear decommissioning projects,” in *Nuclear decommissioning: planning, execution and international experience* (Elsevier), 375–415. doi:10.1533/9780857095336.2.375
- Vichery, C. (2012). “Procédé de recuit protégé appliqué à des nanoparticules d’oxyde de fer: étude des relations structure/propriétés magnétiques,” (Ecole Polytechnique ParisTech). Phd thesis.
- Volk, R., Hübner, F., Hünlich, T., and Schultmann, F. (2018). The future of nuclear decommissioning – a worldwide market potential study. *Energy Policy* 124, 226–261. doi:10.1016/j.enpol.2018.08.014
- Voyshnis, S., Seyeux, A., Zanna, S., Martin-Cabanas, B., Couvant, T., and Marcus, P. (2018). Oxide layer growth on nickel-base alloy surfaces in high temperature water and in o<sub>2</sub> studied by tof-sims with isotopic tracers. *Corros. Sci.* 145, 212–219. doi:10.1016/j.corsci.2018.10.009
- Wang, Y., and Stone, A. T. (2006). Reaction of MnIII,IV (hydr)oxides with oxalic acid, glyoxylic acid, phosphonoformic acid, and structurally-related organic compounds. *Geochimica Cosmochimica Acta* 70, 4477–4490. doi:10.1016/j.gca.2006.06.1548
- Wille, H., and Bertholdt, H. (1998). *Recent developments and experience with the cord uv process*. Japan: Japan Atomic Industrial Forum, Inc.
- Wille, H., Bertholdt, H., and Roumiguere, F. (1997). “Chemical decontamination with the CORD UV process: principle and field experience,” in *Proceedings of 4<sup>th</sup> Regional Meeting Nuclear Energy in Central Europe, Bled, Slovenia, 7 to 10 September 1997*, 199–208.
- Wollast, R., Billen, G., and Duinker, J. C. (1979). Behaviour of manganese in the Rhine and Scheldt estuaries: I. Physico-chemical aspects. *Estuar. Coast. Mar. Sci.* 9, 161–169. doi:10.1016/0302-3524(79)90111-7
- Yatim, S., Zainuddin, N., Mokhtar, N., Syahjidan, H., and Kamsuri, S. (2021). Competitiveness in removing copper, zinc and chromium trivalent in plating industrial effluent by using hydroxide precipitation versus sulphide precipitation. *IOP Conf. Ser. Mater. Sci. Eng.* 1053, 012084. doi:10.1088/1757-899X/1053/1/012084
- Zainuri, M. (2017). Hematite from natural iron stones as microwave absorbing material on X-band frequency ranges. *IOP Conf. Ser. Mater. Sci. Eng.* 196, 012008. doi:10.1088/1757-899X/196/1/012008
- Zhang, R., and Tian, Y. (2020). Characteristics of natural biopolymers and their derivative as sorbents for chromium adsorption: a review. *J. Leather Sci. Eng.* 2, 24. doi:10.1186/s42825-020-00038-9